





## Article

# A Parameter Study of 1D Atmospheric Models of Pulsating AGB Stars

Henry A. Prager<sup>1,2,\*</sup> , Lee Anne M. Willson<sup>3</sup> , Joyce A. Guzik<sup>2</sup> , Michelle J. Creech-Eakman<sup>1</sup>  and Qian Wang<sup>4</sup>

<sup>1</sup> Department of Physics, New Mexico Institute of Mining and Technology, 801 Leroy Place, Socorro, NM 87801, USA; michelle.creecheakman@nmt.edu

<sup>2</sup> Los Alamos National Laboratory, Bikini Atoll Rd., Los Alamos, NM 87545, USA; joy@lanl.gov

<sup>3</sup> Department of Physics, Iowa State University, 2323 Osborn Drive, Ames, IA 50011, USA; lwillson@iastate.edu

<sup>4</sup> Department of Food Science and Human Nutrition, Iowa State University, Food Sciences Bldg, 2312, 536 Farm House Lane, Ames, IA 50011, USA; wangqian@iastate.edu

\* Correspondence: henry.prager@student.nmt.edu

**Abstract:** Using the atmospheric pulsation code written by George Bowen, we have performed a parameter study examining the effects of modifying various parameters of models of oxygen-rich AGB atmospheres pulsating in the fundamental and first-overtone modes. For each pulsation mode, we have examined the effects of adjusting the dust condensation temperature, dust condensation temperature range, pulsation amplitude, dust opacity, and metallicity. Our model grids are generated with the constraint that their luminosities are chosen to span the range of observed mass loss rates at a chosen mass. The dust condensation temperature, pulsation amplitude, and dust opacity have strong effects on the ultimate location and shape of the final model grids in the mass luminosity plane. The mass loss rate evolution of the fundamental and first-overtone mode models show a significant difference in behavior. While the fundamental mode models exhibit the typically assumed power-law relation with mass and luminosity, the first-overtone mode models show significant non-power law behavior at observed mass loss rates. Effectively, models in the first-overtone mode require somewhat higher luminosities to reach the same mass loss rates seen in fundamental mode models of the same mass, consistent with observed AGB stars.

**Keywords:** asymptotic giant branch; evolved stars; giant stars; late-type giant stars; M giant stars; Mira variable stars; pulsating variable stars; stellar mass loss; stellar pulsations; astronomy data modeling



**Citation:** Prager, H.A.; Willson, L.A.M.; Guzik, J.A.; Creech-Eakman, M.J.; Wang, Q. A Parameter Study of 1D Atmospheric Models of Pulsating AGB Stars. *Galaxies* **2024**, *12*, 81.

<https://doi.org/10.3390/galaxies12060081>

Academic Editors: Paolo Ventura, Flavia Dell'Agli and Oscar Straniero

Received: 15 September 2024

Revised: 18 November 2024

Accepted: 18 November 2024

Published: 29 November 2024



**Copyright:** © 2024 by the authors. Licensee MDPI, Basel, Switzerland. This article is an open access article distributed under the terms and conditions of the Creative Commons Attribution (CC BY) license (<https://creativecommons.org/licenses/by/4.0/>).

## 1. Introduction

Mass loss in AGB stars is driven by a pulsation and dust-driven stellar wind during the thermally pulsating (TP-AGB) phase. In this process, pulsations shock the stellar atmosphere, leaving a post-shock cooled region (or, a refrigeration zone), allowing the condensation of dust in the stellar atmosphere. This dust entrains the local gas, and is driven outwards by radiation from the star and the recurring pulsations. This mass loss has been measured to be on the order of  $10^{-7}$  to  $10^{-5} M_{\odot}/\text{yr}$ , leading to the star losing its envelope and becoming a white dwarf. The state of our understanding of this process is reviewed in Höfner and Olofsson [1].

Over the past 30 years, models of the stellar atmosphere have progressively become more detailed. In one dimension, the DARWIN code is the state-of-the-art with detailed calculations for radiative transfer and dust nucleation [2–8]; work is now being conducted to model these atmospheres in 3D [9]. However, as more detailed calculations are incorporated into models, we sacrifice computational speed. With limited computer time, astronomers must have some notion of what the input parameters of the models should be.

For this work, we used the pulsation code written by George Bowen [10]. While incredibly sophisticated and intensive in its time, on modern systems, the code is extremely

fast. This makes it particularly useful for generating numerous large grids of models. Using these grids, we can quantify the effects of adjusting model parameters, clearly demonstrating which parameters have the greatest impact on the properties of resulting models.

## 2. Materials and Methods

The Bowen code is a one-dimensional code that uses an adaptive Lagrangian grid. A piston is placed at the bottom of the grid, located three pressure scale heights below the photosphere, which drives oscillations in the atmosphere. Note that this code does not attempt to model the source of the pulsations, only their effect on the stellar atmosphere. As is typical for these types of models, the pulsation amplitude is increased over several cycles to develop a stable stellar wind. In this model, dust is treated simply, with the opacity of the dust and fraction condensed being convoluted and only the final effect of the dust grains on the model layer being modeled. This prescription makes adjustments to the broad properties of the dust straightforward, but precludes modeling of processes impacting individual grains, such as dust–gas drift; however, these effects become less relevant as the mass loss rate increases, and we are particularly focused on stars with the highest mass loss rates (see Krueger and Sedlmayr [11] and Höfner and Olofsson [1]). The dust opacity in a layer is described by the logistic curve

$$\kappa_D = \kappa_{D,\max} \frac{1}{1 + \exp[(T - T_{\text{con}})/\delta_T]} \quad (1)$$

where  $\kappa_D$  is the dust opacity in a layer,  $\kappa_{D,\max}$  is the maximum dust opacity,  $T$  is the kinetic temperature of the gas,  $T_{\text{con}}$  is the condensation temperature of the dust, and  $\delta_T$  is the range of temperatures that dust can condense; below  $T_{\text{con}} - \delta_T$ , dust is assumed to have condensed, and above  $T_{\text{con}} + \delta_T$  none of the dust is assumed to have condensed. Dust sublimation occurs (so,  $\kappa_D$  decreases) only if the dust reaches radiative equilibrium with the surrounding gas and the equilibrium temperature  $T_{\text{eq}}$  is above the minimum condensation temperature.

$$\kappa_D = \kappa_{D,\max} \frac{1}{1 + \exp[(T_{\text{eq}} - T_{\text{con}})/\delta_T]} \quad (2)$$

This specification means that once dust condenses from the stellar atmosphere, it largely remains condensed, even deep within the stellar atmosphere, leading to a strong pulsation and dust-driven stellar wind. The development of shock waves is extremely important for understanding the evolution of the stellar wind, and is treated carefully through a temperature- and density-dependent relaxation rate, allowing a dynamic transition from mostly isothermal shocks in the deep atmosphere to mostly adiabatic shocks in the outer atmosphere, as suggested by Willson and Hill [12]. For more detail on the physical assumptions, see Bowen [10], or, for full documentation, see Prager [13].

For this project, we used the code to generate grids of atmospheric models across the mass–luminosity plane. Each grid is differentiated by changing the parameters that characterize various physical properties of the model. A full list of the model parameters, a brief description, and the default input values can be found in Table 1. Models are generated starting at  $L = 10^3 L_\odot$  in increments of  $\Delta \log L/L_\odot = 0.05$  until a mass loss rate of  $2 \times 10^{-5} M_\odot/\text{yr}$  is reached. The grids are limited to the observed range of mass loss rates seen in the Large Magellanic Cloud [14,15]. Assuming  $\dot{M} = 2 \times 10^{-5} M_\odot/\text{yr}$  is the maximum mass loss rate, this implies minimum mass loss rates of  $\dot{M} = 10^{-7.4} M_\odot/\text{yr}$  in the fundamental mode and  $\dot{M} = 10^{-7.7} M_\odot/\text{yr}$  in the first-overtone mode.

In this model, stellar mass is removed through the elimination of the outermost layer during the rezoning process, assuming it has a sustained outward flow, at the end of a pulsation cycle. The total amount removed is tracked through the model run; by dividing it by the total number of elapsed cycles, we can determine the average mass loss rate  $\dot{M}$ .

**Table 1.** List of model parameters in the Bowen code. Column 1 notes shorthand names for these parameters, column 2 gives a brief description of the parameter, and column 3 gives a typical value for each parameter. In the case of parameters varied across model grids, these are also the reference values (see Section 2).

Input Parameter	Description	Values
$\log L_0/L_\odot$	Initial Stellar Luminosity	3.0
$\Delta \log L/L_\odot$	Luminosity step	0.05
$u_{\text{amp.}}$	Piston velocity amplitude	2 km/s
$\kappa_g$	Gas opacity	0.0002 cm <sup>2</sup> /g
$\rho_{\text{cx}}$	Gas critical density	10 <sup>-10</sup> g/cm <sup>3</sup>
$q$	Pseudoviscosity Pressure	4 dyn/cm <sup>2</sup>
$n_e/n_H$	Electron-to-Hydrogen Ratio	0.1%
$\kappa_{\text{D,max.}}$	Maximum dust opacity	2 cm <sup>2</sup> /g
$T_{\text{con.}}$	Dust condensation temperature	1450 K
$\delta_T$	Dust condensation temperature range	100 K
$\kappa_W$	Molecular opacity	0.4 cm <sup>2</sup> /g
$T_{\text{con.,W}}$	Molecular condensation temperature	2000 K
$E_{\text{disc.,W}}$	Molecular dissociation energy	43 keV
$\rho_{\text{cx,W}}$	Molecular critical density	1 × 10 <sup>-7</sup> g/cm <sup>3</sup>

### Reference Model and Adjustment Choice

To begin our analysis, we examined two grids of models with the model parameters used in Bowen [10] and with parameters similar to those used in other works (c.f., Bladh et al. [5,7,8], Höfner et al. [16]), one with models pulsating in the fundamental mode and the other in first-overtone mode. All stars in this study are assumed to have an oxygen-rich composition, or spectral type M. The periods and radii are defined by the pulsation–mass–radius and radius–mass–luminosity relations of Trabucchi et al. [17] as appropriate for the pulsation mode and composition, where the C/O ratio has been eliminated as in Prager et al. [18] because it is outside the model’s scope, and the hydrogen fraction is set to  $X = 0.72$  and an assumed metallicity of  $Z = 0.002$ , similar to that of the AGB stars in the Large Magellanic Cloud (see Harris and Zaritsky [19]), not the bulk present metallicity. Note that in Prager et al. [18], the radius–mass–luminosity relation is significantly better constrained for oxygen-rich stars than carbon-rich stars; this is because these relations between parameters become increasingly non-linear at a higher mass, as found by Trabucchi et al. [17]. Therefore, we modeled stars with AGB masses of 0.6, 0.7, 1.0, 1.2, 1.4, 1.7, and 2.0  $M_\odot$ , spanning the range of observed masses for M-type (that is, C/O < 1) AGB stars that have not undergone hot-bottom burning. Note that this carries forward the choice of  $\alpha_{\text{ml}} = 2.0$ . The full list of reference values can be found in Table 1.

Among the parameters in Table 1, the ones with the weakest constraints and strongest expected impact on the output models are the maximum dust opacity  $\kappa_{\text{D,max.}}$ , the dust condensation temperature  $T_{\text{con.}}$ , the phase transition range  $\delta_T$ , the piston amplitude  $u_{\text{amp.}}$ , and the metallicity  $Z$ . Metallicity in particular is expected to have a significant impact on the availability of material to form dust; however, this relation is non-trivial and is further examined in the upcoming final version of this study, Prager et al. [20].

For the remaining parameters, we explored ranges based on the results of several works. Following Höfner [2], the dust opacity is expected to be on the order of a few cm<sup>2</sup>/g, assuming spherically symmetric dust; assuming that greater fractions of the dust condense in each layer or assuming more favorable dust morphologies can increase the dust opacity to establish our upper explored limit of 50 cm<sup>2</sup>/g. In the case of the suspected species in M-type AGB stars, Al<sub>2</sub>O<sub>3</sub> and MgO, their respective condensation temperatures are expected to be around 1000 K, with some range depending on the treatment of nucleation (see Höfner et al. [6] and Bladh et al. [8] for the results of alternative approaches), with values in this range often being used to fit observations (c.f., Ohnaka et al. [21]); we chose to explore the range of 1000 to 1850 K. The piston amplitude is particularly poorly constrained, limited only such that the final observed outflow of the outer atmosphere is on the order of 30 km/s. In real stars, the pulsation-driving region near the photosphere is on the order of a few

km/s; it is often assigned uniformly (c.f., Bladh et al. [7,8], Bowen [10], Fleischer et al. [22]) or occasionally related to the luminosity of the star (c.f. Bowen and Willson [23]). We examined both approaches here, with constant amplitudes noted or expressed through a numerical factor,  $\epsilon$ , defined through energy conservation,

$$u_{\text{amp.}} = \sqrt{2\epsilon \frac{L_* P}{M_{\text{atm.}}}} \quad (3)$$

where  $L_*$  is the mean luminosity of the star,  $P$  is the pulsation period, and  $M_{\text{atm.}}$  is the mass of the stellar material located above the piston. For constant amplitudes, we explored a range of 1 to 8 km/s, with the fundamental mode assumed to be able to pulsate with twice the magnitude of the first overtone mode. For  $\epsilon$ , we investigated a range of 0.01 (1%) to 0.05 (5%).

### 3. Results

With the reference model, we can immediately compare the model output to observation. This will clearly demonstrate if some correction to the models is needed, or if the models we are using are sufficient. This comparison can be seen in Figure 1.

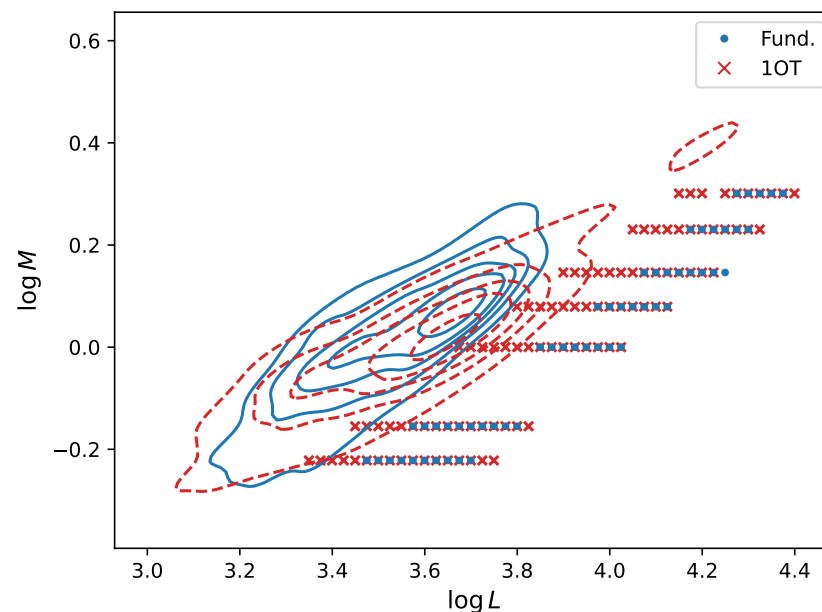


**Figure 1.** This diagram depicts the location of observed AGB stars (contours) and models generated using reference values (markers) in  $\log M$  vs.  $\log L$  in solar units. Solid blue contours depict the location of fundamental mode M-type stars in the LMC and dashed red contours depict the location of first-overtone mode M-type stars in the LMC from Riebel et al. [14]; contours are the percentile of stars included in steps of 20, starting from 90 working inward. Blue dots are fundamental mode M-type star models and red crosses are first-overtone-mode M-type star models within the established mass loss rate ranges.

It is evident that the reference model is not consistent with observed AGB stars. In Section 3.1, we explore the effects of adjusting the parameters outlined in Section 2. In Section 3.2, we determine the shifts in parameters necessary to match observation. Finally, in Section 3.3, we examine the physical differences we are seeing between models pulsating in the fundamental and first-overtone modes.

#### 3.1. Parameter Study

The primary goal of this study was to quantify the effects of adjusting model parameters. In particular, we were interested in the position of the output grids in luminosity–mass

space and the orientation of these grids. For this, we calculated the death line of each grid, as defined in Prager et al. [18]. In short, this line is where the star changes from predominantly growing in luminosity to predominantly losing mass. More technically, this is the turning point where an evolving star reaches a critical mass loss rate  $\dot{M}_{\text{crit.}} = M/t_{\text{ev.}}$ , where  $t_{\text{ev.}}$  is a characteristic  $e$ -folding time for the luminosity,  $10^{6.2}$  yr, which traces a line in  $M$  vs.  $L$  space, or related transformations. We can calculate the shift in position through the changes in the death line luminosity at a reference mass (arbitrarily, we chose  $1 M_{\odot}$ ). The slope of this line is then useful for assessing the orientation of a grid; as shown in Prager et al. [18], the slope is equivalent to the ratio of exponents  $B$  and  $C$  of a power law

$$\log \dot{M} = \log A + B \log L + C \log M, \quad (4)$$

with coefficient  $A$ , and is noted as such here.  $A$ ,  $B$ , and  $C$  are determined through observation; improvements to this formula have been made over several decades, and we will be using the values determined in Prager et al. [18].

In all examined parameters, the effect on adjusting the orientation of the grid varies between a few to nearly 10% in the explored range, as can be seen in Figure 2. This cannot match the uncertainty on the observed ratio in Prager et al. [18] while matching the position of the death line, but we also note that it is weak compared to the effects of the chosen mass loss rate cut-off and resolution of the model grid. Further investigation into more parameters in Prager et al. [20] further addresses this discrepancy. We found that three parameters have notably strong effects on the position of the grid: piston amplitude, dust opacity, and condensation temperature. This is expected given our understanding that AGB stars have a pulsation and dust-driven wind; in these models, increasing these values means having stronger pulsations, more dust, and dust formation at greater depth in the atmosphere. This allows the stars to reach the observed range of mass loss rates (see Section 2) at lower luminosities. The other parameter we adjusted,  $\delta_T$ , has a comparatively small effect. These effects can be seen in Figure 3. The numerical results for this analysis in the fundamental mode can be found in Tables 2 and 3 for the first-overtone mode.

**Table 2.** This table shows the effects of adjusting model parameters ( $X$ ) of M-type AGB stars pulsating in the fundamental mode. The parameters tested are maximum dust opacity  $\kappa_{D,\text{max.}}$ , dust condensation temperature  $T_{\text{con.}}$ , condensation temperature width  $\delta_T$ , velocity amplitude  $u_{\text{amp.}}$ , or piston energy factor  $\epsilon$ . Shifts can be quantified through calculating how the width of the grid changes with adjustments to the specified parameter  $X$  (column 3) and how the location of the grid in LM space changes with respect to  $X$  (column 4).

Parameter ( $X$ )	Test Values	$\frac{d B/C }{d \log X}$	$\frac{d \log L_{DL}}{d \log X}$
$\kappa_{D,\text{max.}}$	0.5, 1, 2, 5, 10, 20, 50 $\text{cm}^2/\text{g}$	−0.020	−0.138
$T_{\text{con.}}$	1000, 1150, 1300, 1450, 1600, 1750 K	0.022	−0.839
$\delta_T$	50, 100, 200, 300, 500 K	0.035	−0.053
$u_{\text{amp.}}$	2, 4, 6, 8 km/s	0.017	−0.350
$\epsilon$	1%, 2%, 3%, 4%, 5%	0.069	−0.127

**Table 3.** This table shows the effects of adjusting model parameters ( $X$ ) of M-type AGB stars pulsating in the first-overtone mode. The constant piston amplitudes tested were halved to keep piston energies consistent between modes. Otherwise, this table follows Table 2.

Parameter ( $X$ )	Test Values	$\frac{d B/C }{d \log X}$	$\frac{d \log L_{DL}}{d \log X}$
$\kappa_{D,\text{max.}}$	0.5, 1, 2, 5, 10, 20, 50 $\text{cm}^2/\text{g}$	−0.008	−0.172
$T_{\text{con.}}$	1000, 1150, 1300, 1450, 1600, 1750, 1850 K	0.112	−1.858
$\delta_T$	50, 100, 200, 300, 500 K	0.109	−0.037
$u_{\text{amp.}}$	1, 2, 3, 4 km/s	0.057	−0.085
$\epsilon$	1%, 2%, 3%, 4%, 5%	0.015	−0.020

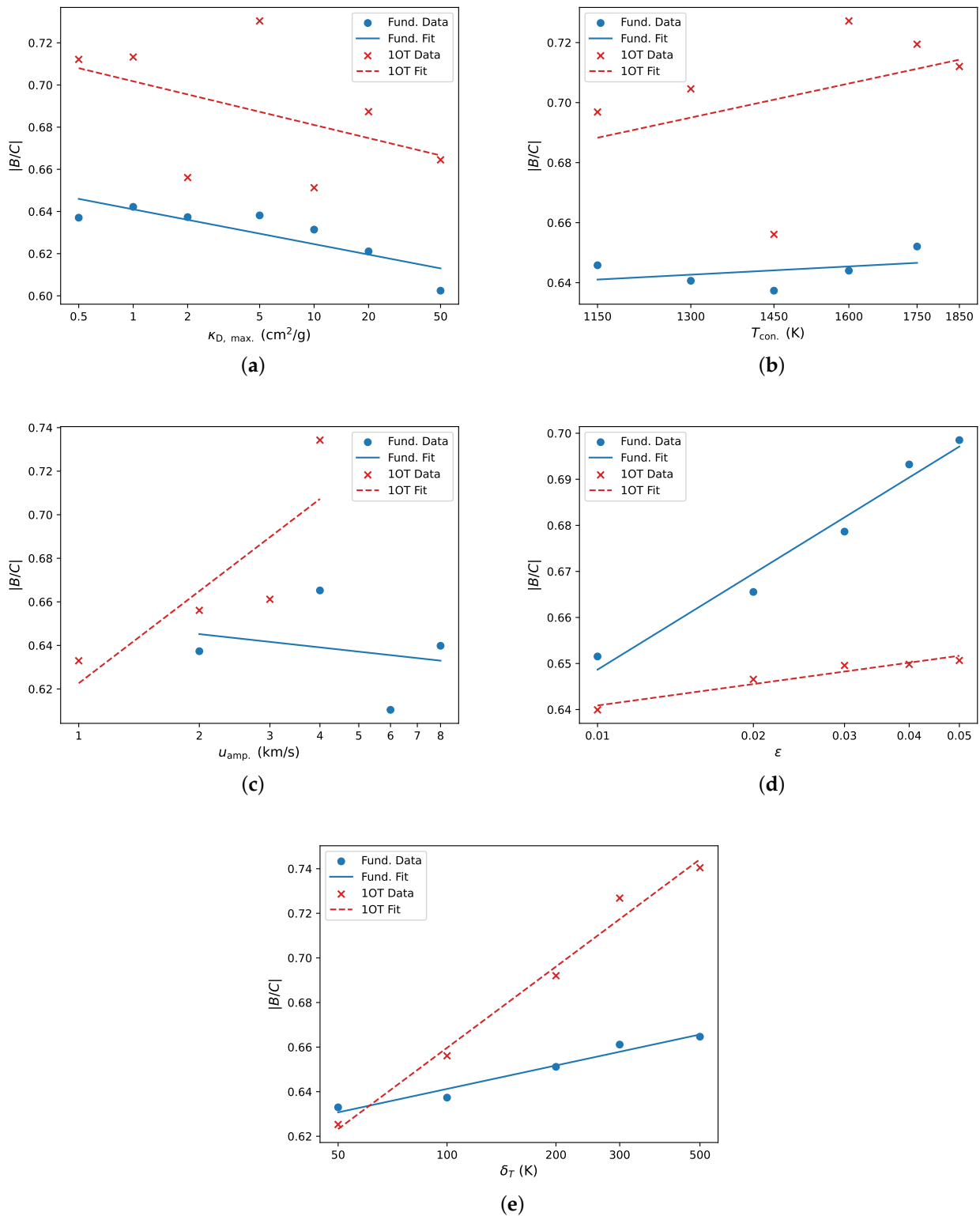


**Figure 2.** These figures depict the effects of adjusting model parameters on the ratio of the power law exponents  $|B/C|$ , and thus the orientation of the model grid. Shifts due to the maximum dust opacity  $\kappa_{D, \max.}$  are found in (a), the dust condensation temperature  $T_{\text{con.}}$  in (b), a constant piston amplitude  $u_{\text{amp.}}$  in (c), the factor  $\epsilon$  from Equation (3) in (d), and the range of condensation and evaporation temperatures  $\delta_T$  in (e). The fundamental mode fit line can be seen in solid blue with individual grids marked by blue dots, and the first-overtone mode fit line can be seen in dashed red with individual model grids marked by red crosses.

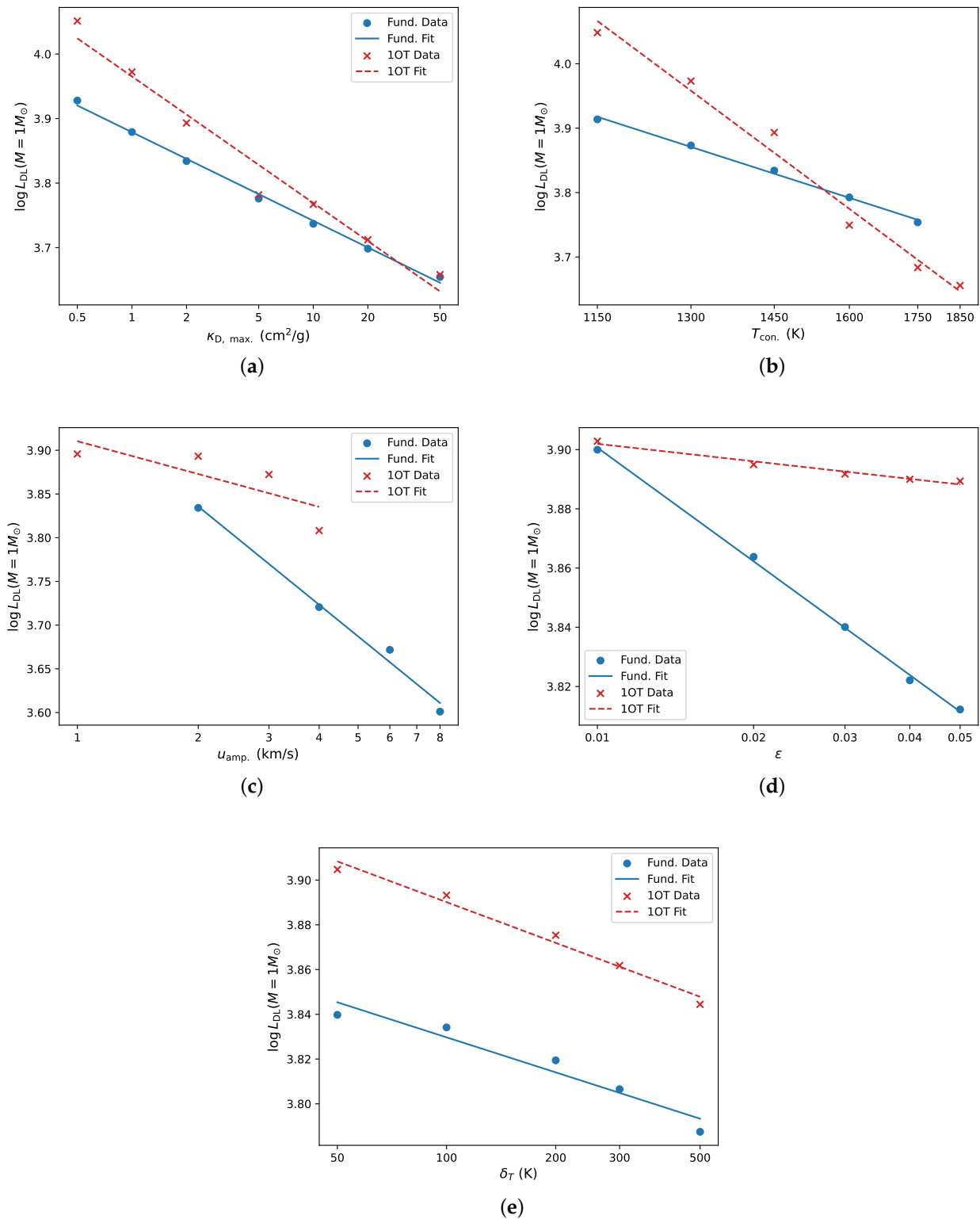


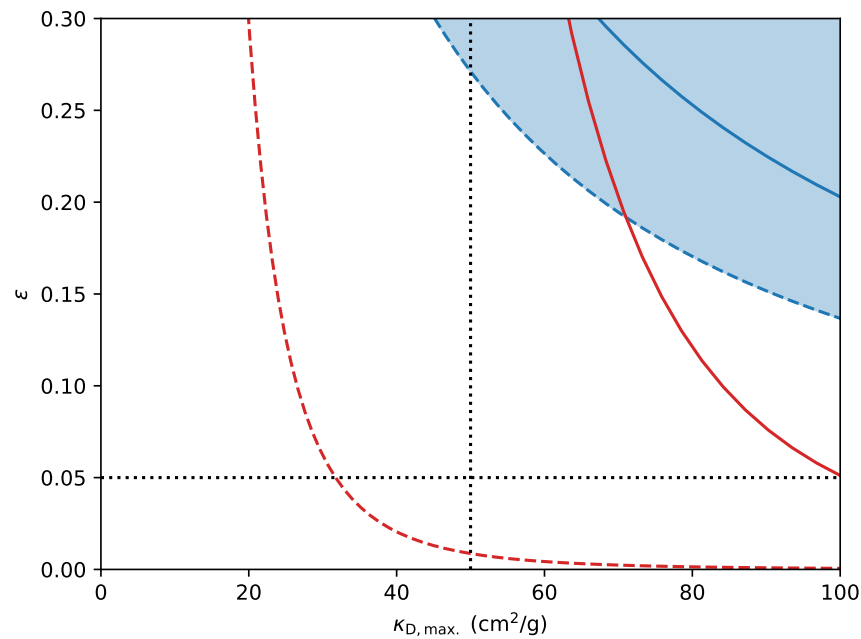
**Figure 3.** These figures depict the effects of adjusting model parameters on the position of the death line, and thus the position of the model grid. Shifts due to the maximum dust opacity  $\kappa_{D, \max.}$  are found in (a), the dust condensation temperature  $T_{con.}$  in (b), a constant piston amplitude  $u_{amp.}$  in (c), the factor  $\epsilon$  from Equation (3) in (d), and the range of condensation and evaporation temperatures  $\delta_T$  in (e). The fundamental mode fit line can be seen in solid blue with individual grids marked by blue dots, and the first-overtone mode fit line can be seen in dashed red with individual model grids marked by red crosses.

### 3.2. Comparison to Observations

Noting Figure 1, the model grids do need some adjustment to match observation. As noted previously, observations are well fit by models with condensation temperatures around 1500 K (c.f., Ohnaka et al. [21]). Given the weak effects of adjusting the temperature range  $\delta_T$ , the maximum dust opacity and pulsation amplitude are the best candidates to adjust to attempt to match model grids with observations. In Prager et al. [18], we determined the location of the death line for the AGB stars in the LMC, showing that the intrinsic spread in these observed sequences of AGB stars is related to the power law that can reproduce them. If we use a Monte Carlo method by randomly assigning the reported errors on the individual data and repeating the analysis, we converge to the errors in Table 4. Noting these errors, we can determine the first-order approximation for the error on the death line position, as defined in Equation (4).

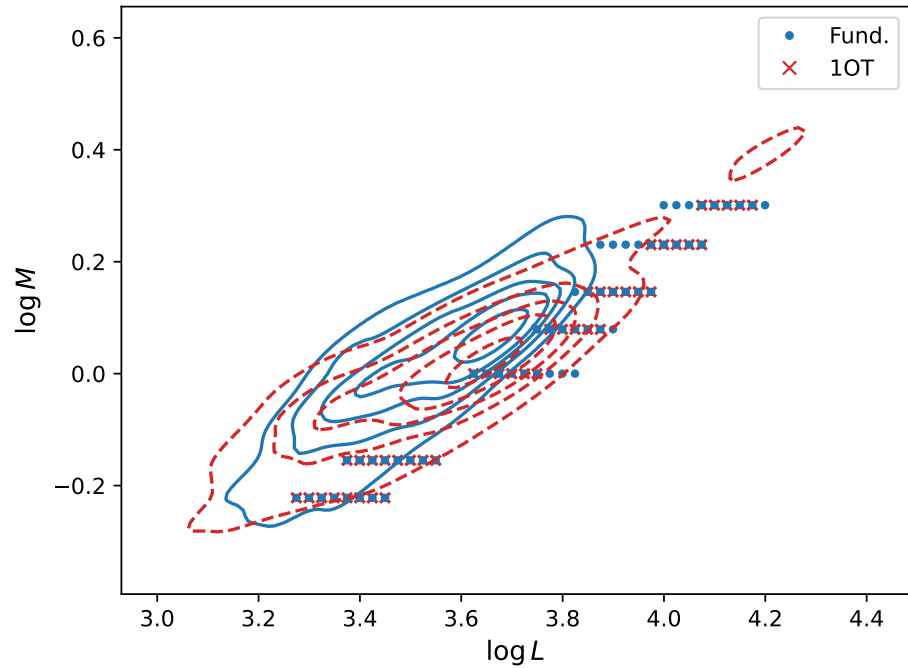
$$\sigma_{\log L, DL} = \frac{(C \pm \sigma_C - 1) \log M}{B \pm \sigma_B} - \frac{(\log t_{ev} + \log A \pm \sigma_{\log A})}{B \pm \sigma_B} - \frac{(C - 1) \log M - (\log t_{ev} + \log A)}{B} \quad (5)$$

Figure 4 depicts the shifts necessary for a model grid to be consistent with the observation, where  $\epsilon = 0.01$  is taken to be the reference value; of the tested values, it produces piston amplitudes that most closely resemble the reference piston amplitude in Table 1. To match the observation, these models require a significant increase to the maximum dust opacity and energy transferred to the piston. The most extreme pair tested was  $\epsilon = 0.05$  and  $\kappa_{D, \max.} = 50 \text{ cm}^2/\text{g}$ , which we can see compared to observations in Figure 5. Further work is being performed to test additional parameters to see if they can account for the discrepancy, or if the required shift cannot be generated in 1D models with current physical assumptions.



**Figure 4.** This figure depicts the necessary change in energy factor  $\epsilon$  or maximum dust opacity  $\kappa_{D, \max.}$  necessary for a grid of models generated using the Bowen atmospheric pulsation code to match the observed population of AGB stars in the LMC. The blue shaded region spans the shifts for the fundamental mode, with the solid curve being the shift, assuming no error in Prager et al. [18], and the dashed lines bounding the maximum spread, as described by Equation (5). The red shaded region and corresponding curves show the same for the first-overtone mode. Note that this figure extends beyond the bounds discussed in Section 2 to show which combination of parameters is implied to replicate the observed range of AGB stars.





**Figure 5.** This figure depicts an extreme (*not physical*) combination of the explored parameters chosen to shift the death line position as close to observations as possible,  $\epsilon = 0.05$  and  $\kappa_{D,\max.} = 50 \text{ cm}^2/\text{g}$ . The contours depict the same data as in Figure 1. Fundamental-mode models are represented by blue dots and first-overtone models are represented by red crosses. The fundamental-mode models have moved closer to the observed population, but are not yet in agreement. While the first-overtone mode models are within error bounds, neither they nor the fundamental mode are as extensive as expected, implying the mass loss rate increases too quickly with luminosity.

**Table 4.** These are the exponents determining the power law formulas  $\log \dot{M} + \log A + B \log L + C \log M$  that best replicate the observed population of AGB stars in the LMC, as found in Prager et al. [18] with the addition of bounds as found through a Monte Carlo estimation of the error.

Pulsation Mode	$\log A$	$B$	$C$	$\Delta \log L_{DL}$	$B/C$
Fundamental	$-35.2 \pm 0.05$	$8.24 \pm 0.04$	$-13.7 \pm 0.07$	$3.58^{+0.05}_{-0.07}$	$0.59 \pm 0.006$
First-Overtone	$-42.8 \pm 0.60$	$10.2 \pm 0.08$	$-20.5 \pm 0.17$	$3.58 \pm 0.03$	$0.50 \pm 0.0002$

### 3.3. Differences Between Pulsation Modes

In Prager et al. [18], we found that AGB stars are undergoing mass loss at nearly the same ranges of masses and luminosities in both the fundamental and first-overtone mode, with the fundamental mode extending to a somewhat higher mass loss rate than the first-overtone mode. This suggests that both are undergoing significant mass loss, and the switch to the fundamental mode does not necessitate passing the death line. Therefore, modeling stars pulsating in the first-overtone mode is necessary to understand the full behavior of these stars.

Preliminary investigations into the cause of this difference suggests there is a correlation with the acoustic properties of the stars. The acoustic cut-off period, the inverse of the acoustic cut-off frequency as described in Jiménez et al. [24], is defined as

$$P_{ac} \equiv \frac{2c_s}{g} = \frac{2H}{c_s} = \frac{2}{g} \sqrt{\frac{5}{3} \frac{R_{\text{gas}}}{M_{\text{mol}} T}} \quad (6)$$

where  $g$  is the local acceleration due to gravity,  $c_s$  is the local sound speed,  $H$  is the local pressure scale height,  $R_{\text{gas}}$  is the gas constant,  $M_{\text{mol}}$  is the molar mass of the local gas, and  $T$  is the local temperature. Waves with periods below the acoustic cut-off period can freely

pass through a change in the medium, while those above it are internally reflected. In the fundamental mode, stars pulsate slower than the acoustic cut-off; in higher modes, it is always faster than this cut-off. This can be seen in Figure 6.

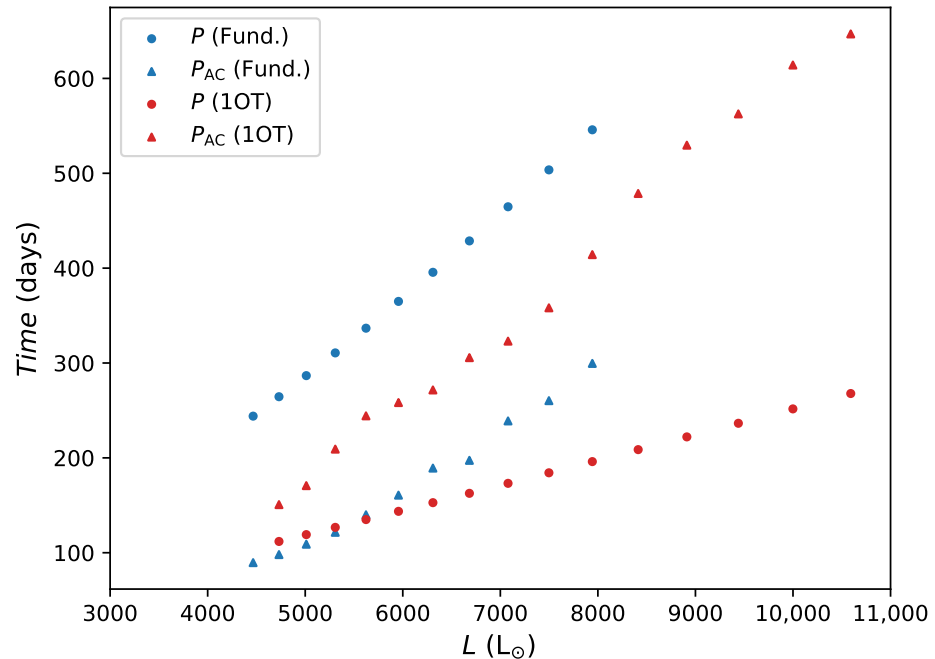


**Figure 6.** Comparisons of pulsation period  $P$  to acoustic cut-off period  $P_{ac}$  in AGB atmospheres of a  $1 M_{\odot}$  star, as a function of luminosity. Blue compares these in the fundamental mode while red compares these in the first-overtone mode. Dots track the pulsation period of the modeled stars, and triangles track the acoustic cut-off period at the photosphere for the modeled stars. The acoustic cut-off period varies between modes due to differences in the effective scale height—the initial  $e$ -folding distance in the dynamic atmosphere—between the different pulsation modes.

If the acoustic cut-off period is related to the source of the difference between modes, then we should see (1) significant differences in the propagation of shock waves between pulsation modes and (2) a correlation between the mass loss rate and the ratio of the period and acoustic cut-off period. The location of shock waves is recorded throughout the modeling process, and an example for a star of  $M = 1 M_{\odot}$  and  $L = 6309 L_{\odot}$  is shown in Figure 7; by default, in the program, a shock is said to be present if the ratio of the pseudoviscosity pressure  $P_Q$  to the gas pressure  $P_G$  in a layer is greater than or equal to 0.10. We can see that shock waves propagate to much greater distances above the surface of the star in the fundamental mode.

The correlation between mass loss rate and the ratio of the period and acoustic cut-off period can be seen in Figure 8; this correlation is strong, but the ratio of the period to acoustic cut-off period alone does not capture the total behavior. There are also effects we have not determined the source of at this time, such as the change in which mode has higher mass loss rates at different luminosities. The results from further investigation will be in an upcoming study, i.e., Prager et al. [25].

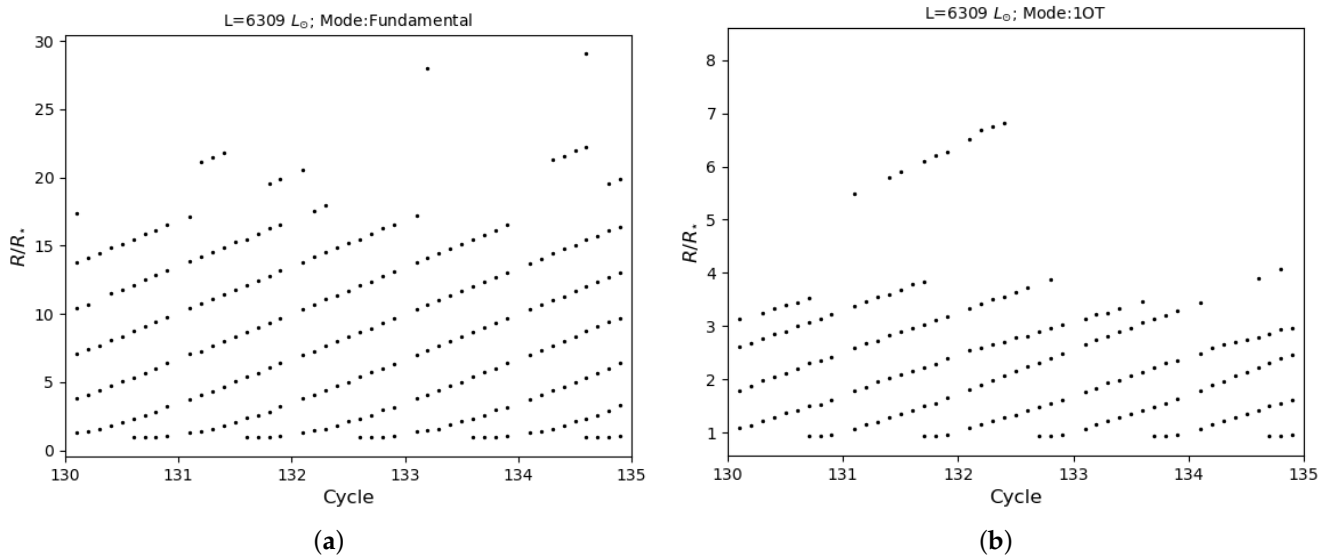


**Figure 7.** These figures depict locations of shock fronts relative to the stellar radius ( $R/R_*$ ) in  $M = 1 M_\odot$ ,  $L = 6309 L_\odot$  AGB atmospheres. (a) displays these in the fundamental mode, (b) displays these in the first-overtone mode. Note that these models share an RML relation (see Section 2) and are thus the same mean radius, but have different cycle time scales due to differences in their pulsation period. These models are evaluated to a distance of over 80 stellar radii, with some variation as models are rezoned (see Bowen [10] for details).

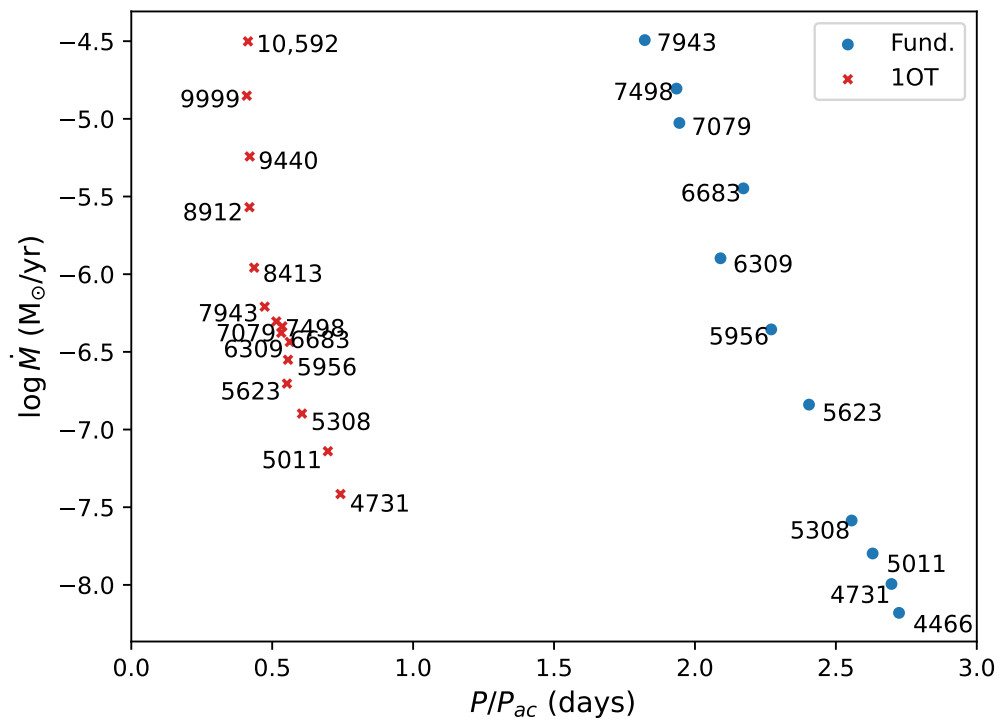


**Figure 8.** This figure demonstrate the inverse correlation between the mass loss rate  $\dot{M}$  (y-axis) and  $P/P_{ac}$  (x-axis) in AGB atmospheres of  $1 M_\odot$  models assuming the reference parameters in Table 1. Blue dots are the fundamental mode models and red crosses are the first-overtone mode models. This plot is limited to models that fall within the observed mass loss rate range (see Section 2). The luminosity of each model in solar units is included in the plot; (4466, 4731, 5011, 5308, 5623, 5956, 6309, 6683, 7079, 7498, 7943) is the fundamental mode set and (4731, 5011, 5308, 5623, 5956, 6309, 6683, 7079, 7498, 7943, 8413, 8912, 9440, 9999, 10,592) is the first-overtone mode set.

#### 4. Discussion

Using the atmospheric pulsation code written by George Bowen [10], we have examined the effects of adjusting various model parameters, explored what changes are necessary to bring these 1D models into agreement with observations, and what is the source of the observed difference between mass loss rates in the fundamental and first-overtone modes. For the first part of this study, we demonstrated that, as expected for a pulsation and dust driven wind, the parameters that control the strength of this wind have the greatest impact on mass loss. As can be seen in Tables 2 and 3, the strongest factor is the location of the primary dust condensation layer, so it is critical that we understand the species that constitute AGB dust and their properties in the atmospheric environment. In both the fundamental and first-overtone modes, we can see the next most important factors are the dust opacity and piston amplitudes. In the case of the former, we can reiterate the importance of understanding dust formation in these stellar atmospheres. In the case of the piston amplitude, we see that the adjustment effects are very strong in the fundamental mode, with significant differences apparent depending on how the piston is treated relative to the stellar luminosity. It appears that understanding the piston mechanism is a critical next step in improving models of stellar atmospheres, which will require models of the pulsation layer in the stellar interior.

In the second part of this study, we assumed that we have a relatively good understanding of the dust chemistry of these stars, and focused on what shifts in dust opacity and piston strength are needed to replicate observed populations of AGB stars. In models, a reasonable dust opacity is on the order of a few  $\text{cm}^2/\text{g}$  with a piston amplitude on the order of a few km/s. We needed dust opacities an order of magnitude larger than this and piston amplitudes nearly twice as large. This is unphysical.

It is possible that more detailed physics could account for the difference, but the most recent results using the DARWIN code [7,8] show that 1D models still require luminosities outside the observed range to reach observed mass loss rates, with less adjustment needed as the effective temperature is increased. This suggests that the change in the models needed to reach agreement with observations is more likely an effect that can only be accounted for with a better understanding of the piston and its driving mechanism, by better understanding dust, by better constraining the radius–mass–luminosity relation, and by taking into account the behavior of the stellar atmosphere in three dimensions.

As the final part of this study, we have begun examining the source of the difference in mass loss rate behavior between the fundamental and first-overtone modes. This is motivated by the results of Prager et al. [18], showing that large mass loss rates are achieved in both the fundamental and first-overtone modes at similar ranges of mass and luminosity. These models suggest a correlation between mass loss rate development and the acoustic properties of AGB stars, where shock waves generated in the fundamental mode are able to freely propagate in the atmosphere but are restricted in the first-overtone mode. This interpretation seems to be consistent with observations and the relative ineffectiveness of increasing the piston amplitude in the first-overtone mode compared to the fundamental mode, but more work is needed.

The final version of parts one and two of this study will be submitted in the near future. Part three will be submitted for review subsequently.

**Author Contributions:** Conceptualization, H.A.P., L.A.M.W., J.A.G. and M.J.C.-E.; methodology, H.A.P., L.A.M.W. and J.A.G.; software, H.A.P., J.A.G. and Q.W.; validation, H.A.P., L.A.M.W., J.A.G. and M.J.C.-E.; formal analysis, H.A.P.; investigation, H.A.P., L.A.M.W., J.A.G. and M.J.C.-E.; resources, J.A.G.; data curation, H.A.P.; writing—original draft preparation, H.A.P.; writing—review and editing, H.A.P., L.A.M.W., J.A.G. and M.J.C.-E.; visualization, H.A.P.; supervision, L.A.M.W., J.A.G. and M.J.C.-E.; project administration, L.A.M.W. and J.A.G.; funding acquisition, J.A.G. All authors have read and agreed to the published version of the manuscript.

**Funding:** This research was funded by the New Mexico Space Grant Consortium and Los Alamos National Laboratory, managed by Triad National Security, LLC for the U.S. DOE's NNSA, Contract # 89233218CNA000001.

**Data Availability Statement:** The data presented in this study are available on request from the corresponding author due to planned submission of the completed analysis at a later date.

**Acknowledgments:** Additional mentorship at Los Alamos National Laboratory has been provided by Katherine Mussack. This work has made use of the NumPy library [26], the SciPy library [27], IPython software package [28], the matplotlib library for publication quality graphics [29], and the Scikit-learn library [30].

**Conflicts of Interest:** The authors declare no conflicts of interest.

## Abbreviations

The following abbreviations are used in this manuscript:

AGB	Asymptotic Giant Branch
LMC	Large Magellanic Cloud
DARWIN	Dynamic Atmosphere and Radiation-driven Wind models based on Implicit Numerics

## References

- Höfner, S.; Olofsson, H. Mass loss of stars on the asymptotic giant branch. Mechanisms, models and measurements. *Astron. Astrophys. Rev.* **2018**, *26*, 1. [[CrossRef](#)]
- Höfner, S. Winds of M-type AGB stars driven by micron-sized grains. *Astron. Astrophys.* **2008**, *491*, L1–L4. [[CrossRef](#)]
- Bladh, S.; Höfner, S. Exploring wind-driving dust species in cool luminous giants. I. Basic criteria and dynamical models of M-type AGB stars. *Astron. Astrophys.* **2012**, *546*, A76. [[CrossRef](#)]
- Bladh, S.; Höfner, S.; Nowotny, W.; Aringer, B.; Eriksson, K. Exploring wind-driving dust species in cool luminous giants. II. Constraints from photometry of M-type AGB stars. *Astron. Astrophys.* **2013**, *553*, A20. [[CrossRef](#)]
- Bladh, S.; Höfner, S.; Aringer, B.; Eriksson, K. Exploring wind-driving dust species in cool luminous giants. III. Wind models for M-type AGB stars: Dynamic and photometric properties. *Astron. Astrophys.* **2015**, *575*, A105. [[CrossRef](#)]
- Höfner, S.; Bladh, S.; Aringer, B.; Ahuja, R. Dynamic atmospheres and winds of cool luminous giants. I. Al<sub>2</sub>O<sub>3</sub> and silicate dust in the close vicinity of M-type AGB stars. *Astron. Astrophys.* **2016**, *594*, A108. [[CrossRef](#)]
- Bladh, S.; Liljegren, S.; Höfner, S.; Aringer, B.; Marigo, P. An extensive grid of DARWIN models for M-type AGB stars. I. Mass-loss rates and other properties of dust-driven winds. *Astron. Astrophys.* **2019**, *626*, A100. [[CrossRef](#)]
- Bladh, S.; Eriksson, K.; Marigo, P.; Liljegren, S.; Aringer, B. Carbon star wind models at solar and sub-solar metallicities: A comparative study. I. Mass loss and the properties of dust-driven winds. *Astron. Astrophys.* **2019**, *623*, A119. [[CrossRef](#)]
- Höfner, S.; Bladh, S.; Aringer, B.; Eriksson, K. Dynamic atmospheres and winds of cool luminous giants. II. Gradual Fe enrichment of wind-driving silicate grains. *Astron. Astrophys.* **2022**, *657*, A109. [[CrossRef](#)]
- Bowen, G.H. Dynamical Modeling of Long-Period Variable Star Atmospheres. *Astrophys. J.* **1988**, *329*, 299. [[CrossRef](#)]
- Krueger, D.; Sedlmayr, E. Two-fluid models for stationary dust driven winds. II. The grain size distribution in consideration of drift. *Astron. Astrophys.* **1997**, *321*, 557–567.
- Willson, L.A.; Hill, S.J. Shock wave interpretation of emission lines in long period variable stars. II. Periodicity and mass loss. *Astrophys. J.* **1979**, *228*, 854–869. [[CrossRef](#)]
- Prager, H. Studies of Mass-Loss Rates and Stellar Atmospheres on the Asymptotic Giant Branch. Ph.D. Thesis, New Mexico Institute of Mining and Technology, Socorro, NM, USA, 2023.
- Riebel, D.; Meixner, M.; Fraser, O.; Srinivasan, S.; Cook, K.; Vihj, U. Infrared Period-Luminosity Relations of Evolved Variable Stars in the Large Magellanic Cloud. *Astrophys. J.* **2010**, *723*, 1195–1209. [[CrossRef](#)]
- Riebel, D.; Srinivasan, S.; Sargent, B.; Meixner, M. The Mass-loss Return from Evolved Stars to the Large Magellanic Cloud. VI. Luminosities and Mass-loss Rates on Population Scales. *Astrophys. J.* **2012**, *753*, 71. [[CrossRef](#)]
- Höfner, S.; Gautschi-Loidl, R.; Aringer, B.; Jørgensen, U.G. Dynamic model atmospheres of AGB stars. III. Effects of frequency-dependent radiative transfer. *Astron. Astrophys.* **2003**, *399*, 589–601. [[CrossRef](#)]
- Trabucchi, M.; Wood, P.R.; Montalbán, J.; Marigo, P.; Pastorelli, G.; Girardi, L. Modelling long-period variables - I. A new grid of O-rich and C-rich pulsation models. *Mon. Not. R. Astron. Soc.* **2019**, *482*, 929–949. [[CrossRef](#)]
- Prager, H.A.; Willson, L.A.; Marengo, M.; Creech-Eakman, M.J. Relation of Observable Stellar Parameters to Mass-loss Rate of AGB Stars in the LMC. *Astrophys. J.* **2022**, *941*, 44. [[CrossRef](#)]
- Harris, J.; Zaritsky, D. The Star Formation History of the Large Magellanic Cloud. *Astron. J.* **2009**, *138*, 1243–1260. [[CrossRef](#)]

20. Prager, H.A.; Willson, L.A.M.; Guzik, J.A.; Creech-Eakman, M.J.; Wang, Q. A Parameter Study of 1D Atmospheric Models of Pulsating AGB Stars: I. Model Properties and Effects on Wind Development. 2025. *Journal to be decided in Preparation*.
21. Ohnaka, K.; Weigelt, G.; Hofmann, K.H. Clumpy dust clouds and extended atmosphere of the AGB star W Hydrae revealed with VLT/SPHERE-ZIMPOL and VLTI/AMBER. II. Time variations between pre-maximum and minimum light. *Astron. Astrophys.* **2017**, *597*, A20. [[CrossRef](#)]
22. Fleischer, A.J.; Gauger, A.; Sedlmayr, E. Circumstellar dust shells around long-period variables. I. Dynamical models of C-stars including dust formation, growth and evaporation. *Astron. Astrophys.* **1992**, *266*, 321–339.
23. Bowen, G.H.; Willson, L.A. From wind to superwind—The evolution of mass-loss rates for Mira models. *Astrophys. J. Lett.* **1991**, *375*, L53–L56. [[CrossRef](#)]
24. Jiménez, A.; García, R.A.; Pallé, P.L. The Acoustic Cutoff Frequency of the Sun and the Solar Magnetic Activity Cycle. *Astrophys. J.* **2011**, *743*, 99. [[CrossRef](#)]
25. Prager, H.A.; Willson, L.A.M.; Guzik, J.A.; Creech-Eakman, M.J.; Wang, Q. A Parameter Study of 1D Atmospheric Models of Pulsating AGB Stars: II. Relations Between Pulsation Mode and Mass-Loss Rate Evolution. 2025. *Journal to be decided in Preparation*.
26. Harris, C.R.; Millman, K.J.; van der Walt, S.J.; Gommers, R.; Virtanen, P.; Cournapeau, D.; Wieser, E.; Taylor, J.; Berg, S.; Smith, N.J.; et al. Array programming with NumPy. *Nature* **2020**, *585*, 357–362. [[CrossRef](#)]
27. Virtanen, P.; Gommers, R.; Oliphant, T.E.; Haberland, M.; Reddy, T.; Cournapeau, D.; Burovski, E.; Peterson, P.; Weckesser, W.; Bright, J.; et al. SciPy 1.0: Fundamental Algorithms for Scientific Computing in Python. *Nat. Methods* **2020**, *17*, 261–272. [[CrossRef](#)]
28. Pérez, F.; Granger, B.E. IPython: A System for Interactive Scientific Computing. *Comput. Sci. Eng.* **2007**, *9*, 21–29. [[CrossRef](#)]
29. Hunter, J.D. Matplotlib: A 2D graphics environment. *Comput. Sci. Eng.* **2007**, *9*, 90–95. [[CrossRef](#)]
30. Pedregosa, F.; Varoquaux, G.; Gramfort, A.; Michel, V.; Thirion, B.; Grisel, O.; Blondel, M.; Prettenhofer, P.; Weiss, R.; Dubourg, V.; et al. Scikit-learn: Machine Learning in Python. *J. Mach. Learn. Res.* **2011**, *12*, 2825–2830.

**Disclaimer/Publisher’s Note:** The statements, opinions and data contained in all publications are solely those of the individual author(s) and contributor(s) and not of MDPI and/or the editor(s). MDPI and/or the editor(s) disclaim responsibility for any injury to people or property resulting from any ideas, methods, instructions or products referred to in the content.